

## Article

# Silica Aerogel-Rubber Composite: A Sustainable Alternative for Buildings' Thermal Insulation

Patrícia Alves \* , Diogo Azeiteiro Dias and Ana Dora Rodrigues Pontinha \* 

University of Coimbra, Chemical Process Engineering and Forest Products Research Centre, Department of Chemical Engineering, Rua Silvio Lima, 3030-790 Coimbra, Portugal

\* Correspondence: palves@eq.uc.pt (P.A.); dora\_pontinha@hotmail.com (A.D.R.P.)

**Abstract:** Silica aerogel composites with recycled tire rubber have been synthesized and evaluated for their potential use for thermal protection in buildings. The present work describes for the first time the preparation of silica-based aerogel composites containing recycled rubber tires reinforced with polyvinyl butyral (PVB) by hot pressing. The developed composite was extensively characterized regarding its physical, morphological, thermal and mechanical features, and the results showed their properties were relevant, leading to composites with different properties/performances. The obtained bulk density values were satisfactory, down to  $474 \text{ kg}\cdot\text{m}^{-3}$ , and very good thermal properties were achieved, namely, thermal conductivity as low as  $55 \text{ mW}\cdot\text{m}^{-1}\cdot\text{K}^{-1}$  for composites with silica aerogel, recycled tire rubber and PVB. The most promising composites were those based on low bulk density and thermal conductivity values, and they were thermally stable, indicating their suitability for thermal insulation applications.

**Keywords:** silica aerogels; sol-gel; recycled tire rubber; thermal insulation buildings



**Citation:** Alves, P.; Dias, D.A.; Pontinha, A.D.R. Silica Aerogel-Rubber Composite: A Sustainable Alternative for Buildings' Thermal Insulation. *Molecules* **2022**, *27*, 7127. <https://doi.org/10.3390/molecules27207127>

Academic Editor: Igor Djerdj

Received: 20 September 2022

Accepted: 17 October 2022

Published: 21 October 2022

**Publisher's Note:** MDPI stays neutral with regard to jurisdictional claims in published maps and institutional affiliations.



**Copyright:** © 2022 by the authors. Licensee MDPI, Basel, Switzerland. This article is an open access article distributed under the terms and conditions of the Creative Commons Attribution (CC BY) license (<https://creativecommons.org/licenses/by/4.0/>).

## 1. Introduction

Silica-based aerogels are popular in terms of production volume and real-world applications [1]. They have many unique and favorable properties due to their nonporous structural nature [2]. Silica aerogels have received great attention due to some of their properties such as very high pore volume (>90%) and a usually mesoporous network, which provide a very high specific surface area ( $500\text{--}1200 \text{ m}^2 \text{ g}^{-1}$ ) [3], low density ( $\sim 0.03\text{--}0.3 \text{ g}\cdot\text{cm}^{-3}$ ) [4], low thermal conductivity ( $12\text{--}25 \text{ m W}\cdot\text{m}^{-1}\cdot\text{K}^{-1}$ ), ultra-low dielectric constant ( $k = 1.0\text{--}2.0$ ) and low refractive index ( $\sim 1.05$ ) [5,6]. The very low thermal conductivity [2,7] of silica aerogels, associated with nonflammable characteristics, make them suitable materials for thermal insulation systems. However, they have limitations in their mechanical strength and are complex to process without causing fractures in the final material [8]. Different approaches have been explored to improve the mechanical properties of silica aerogels [9], such as structural reinforcement using flexible silica precursors in silica gel backbone [10,11], dispersing fibers in the initial sol of silica aerogel [12] and conformal coating of silica backbone by surface cross-linking with a polymer [13–15].

Due to their unusual physical and chemical features, aerogels have gained great interest, especially for energy-efficient retrofitting solutions for buildings [16]. Aerogels are a state-of-the-art thermal insulation solution with great potential at the moment [5,17–20]. A common passive strategy for the reduction in energy consumption is the incorporation of thermal insulation materials in buildings' envelopes [8,21,22].

On the other hand, the use of discarded tires in the construction industry is an economical and sustainable solution to meet future environmental challenges. The disposal of waste tires to landfills creates serious environmental problems due to the leaching of harmful and toxic elements into the surrounding ecosystem.

In the last decade, there has been a growth in the number of tires discarded as end-of-life tires (ELTs) [23], which leads to serious environmental problems. Approximately

70–80% of the total mass of the tires is vulcanized rubber, and their disposal is an issue, as they are nonbiodegradable and cannot be reprocessed in a simple process such as the thermoplastic materials remaining in the landfills [23–25]. Recycled rubber often lacks the correct balance of disulfide bridges between polymer chains, which are normally formed during the vulcanization stage [26], and the rubber can enter an “overcure” phase, causing it to have a lower tensile strength [27]. In order to ameliorate this problem, polymers are often added.

Polyvinyl butyral (PVB) is an interesting polymer with outstanding mechanical properties and excellent optical clarity [28]. The static mechanical property of PVB has significant deformability and is sensitive to strain rate and temperature [29].

In this work, motivated by the environmental problems caused by ELTs, the goal was to develop a composite of aerogel, recycled tire rubber waste and PVB using the hot-pressing technique. A comparative study on the influence of the different components on the physicochemical, thermal and mechanical features of the resulting composites was carried out. Due to its low thermal conductivity and good mechanical resistance, the aerogel-based composite has the potential for thermal insulation applications.

## 2. Results and Discussion

Since the main goal of this study is to evaluate the influence of aerogel, recycled tire rubber and polymer on the properties of composites, several characterization techniques were employed.

### 2.1. Chemical Characterization

The ATR-FTIR spectra of the different components of the composite, PVB, aerogel and rubber, and two different composites are presented in Figure 1.

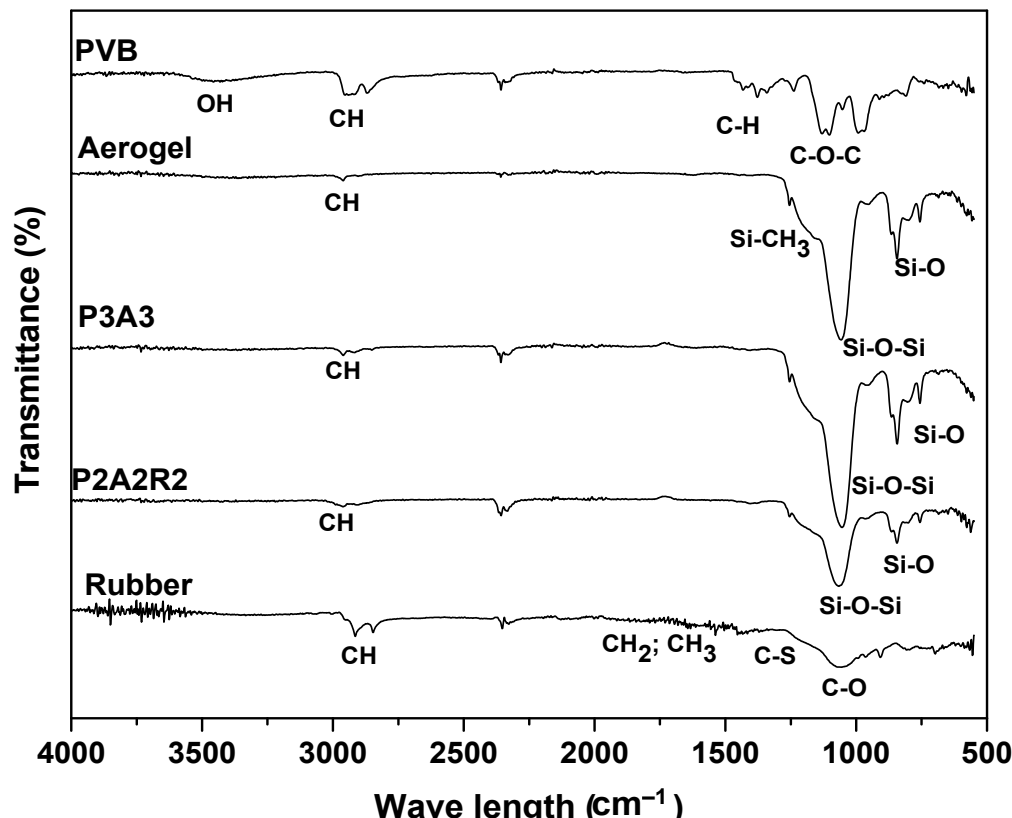


**Figure 1.** FTIR spectra for PVB, aerogel, rubber and different aerogel composites: P3A3 (PVB and aerogel composite) and P2A2R2 (PVB, aerogel and rubber composite).

All infrared spectra presented in Figure 1 show a series of bands in the 2980–2850  $\text{cm}^{-1}$  range assigned to the C–H symmetric and antisymmetric stretching vibrations of  $\text{CH}_3$  and  $-\text{CH}_2$  groups [30]. These bands are more evident for PVB and rubber spectra due to their hydrophobicity. Other typical bands at 1377  $\text{cm}^{-1}$  and 1463  $\text{cm}^{-1}$  ascribed to  $-\text{CH}_3$  symmetric deformation vibrations and bending deformation are also present [31], especially in the PVB spectrum.

The O–H band observed at 3600  $\text{cm}^{-1}$  in PVB is due to the predominance of hydroxyl groups (major), butyral and (less) acetyl groups in its composition [32]. In addition, a band at 1132  $\text{cm}^{-1}$ , which corresponds to the C–O–C butyral ring stretching is a typical band of PVB [31].

The rubber sample spectrum shows symmetric stretching of C–O–C and twisting of  $-\text{CH}_2-$  at 1080  $\text{cm}^{-1}$  and symmetric C–S–C group stretching vibrations in the two C–S bonds at 1250  $\text{cm}^{-1}$ . It is also possible to perceive the deformation of  $-\text{CH}_2-$  and rocking of  $-\text{CH}_3$  and asymmetric deformation of  $-\text{CH}_3$  in the 1500–1700  $\text{cm}^{-1}$  range [33,34].

For all the silica aerogels samples, it is possible to observe the stretching vibrations bands from Si–O–Si bonds of the  $\text{SiO}_2$  network: near 755  $\text{cm}^{-1}$  (symmetric) and 1055  $\text{cm}^{-1}$  (asymmetric), which are attributed to different modes of O–Si–O and Si–O vibration [35]. Regarding the  $-\text{CH}_3$  groups resulting from the sialylation, a band can be found at 2960  $\text{cm}^{-1}$ , corresponding to the symmetric stretching vibration of C–H from methyl groups.

Observing the spectra of composites P3A3 and P2A2R2, it can be seen that they are similar with bands at 3000  $\text{cm}^{-1}$ , 2300  $\text{cm}^{-1}$  and 1000  $\text{cm}^{-1}$ , despite the fact that one of the composites has rubber in its composition (P2A2R2). The presence of rubber was not possible to be confirmed based on the FTIR spectra. Both spectra are more similar to the aerogel spectrum, which might be explained by the fact that the ATR-FTIR analysis only detects the composition at the surface of the composite and, since it is not homogeneous (is a mixture of the three components) it may be detecting a section with more aerogel than rubber or polymer. It should also be noted that, in the composite, many peaks overlap, and hence they cannot be properly identified.

## 2.2. Structural and Morphological Features

Thermogravimetry analysis (TGA) was performed to evaluate the thermal stability of the materials used since high temperatures were employed in the composites processing procedure (around 150 °C).

PVB TGA shown in Figure 2a displays a slight mass loss around 100 °C, resulting from the loss of residual water present in the sample. PVB showed good thermal stability, starting to degrade only at 377 °C, and presented only one step of degradation.

From Figure 2b, it is possible to observe that rubber presents good thermal stability, with an initial decomposition temperature of 331 °C. Until 250 °C, a weight loss of 4.3% was detected, which is probably due to the thermal degradation of the remaining plasticizer portions presented in the rubber [36].

Figure 2c shows a weight loss of silica aerogels near 60 °C. This is the result of the evaporation of entrapped  $\text{H}_2\text{O}$  and alcoholic groups from hydrophilic silica aerogels as a result of the condensation reactions of Si–OH and Si( $\text{OC}_2\text{H}_5$ ) groups [37].

## 2.3. Surface Hydrophobicity

The water contact angle gives information about the surface hydrophilic/hydrophobic character, which strongly influences the interaction between the material and its surroundings (such as other materials or moisture). The results presented in Table 1 show the obtained values of the static water contact angle.

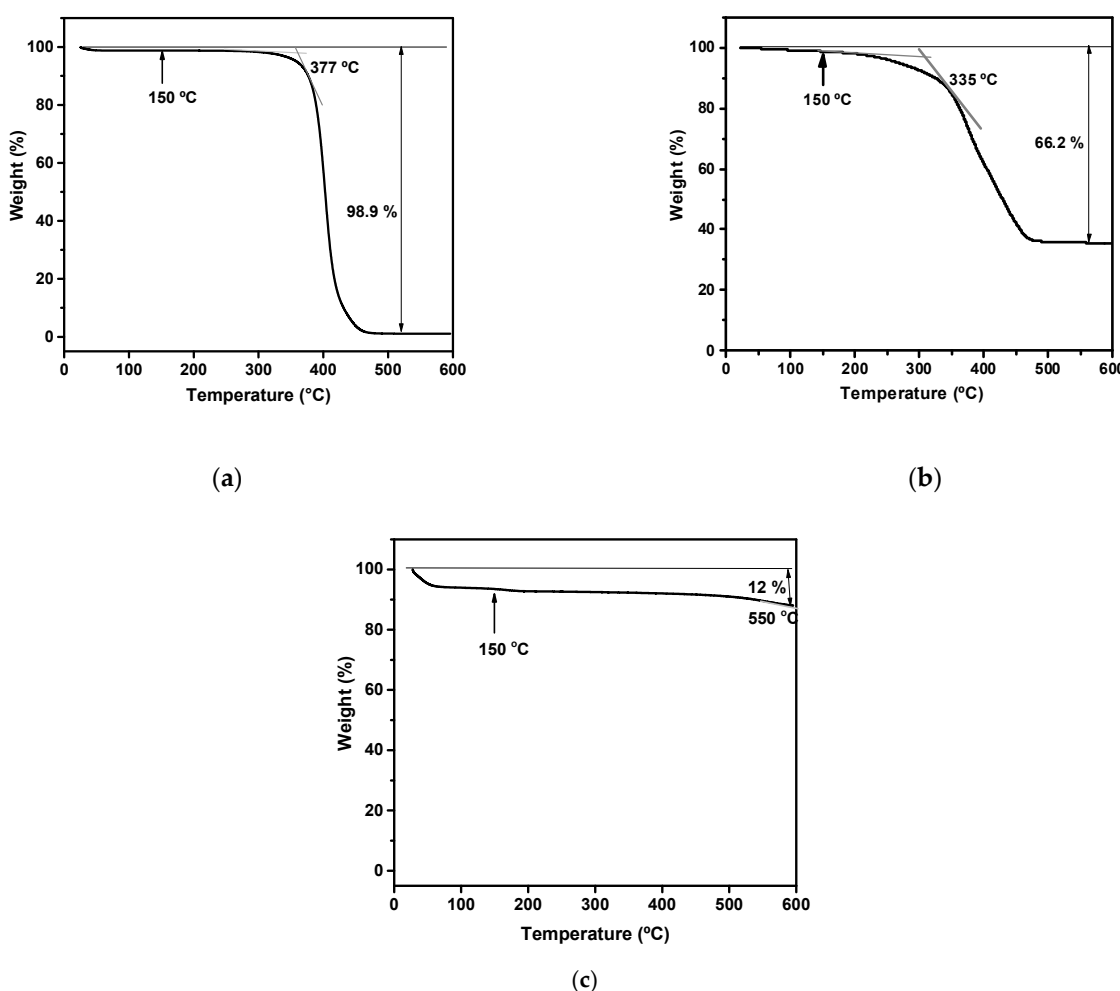


**Figure 2.** TGA traces of: (a) PVB; (b) rubber; (c) silica aerogel.

**Table 1.** Static water contact angle of different samples.

Samples/Composites	Water Contact Angle (°)
P6	116.7 ± 2.4
P3A3	151.7 ± 4.6
P2A4	156.8 ± 3.1
P3R1A2	158.8 ± 2.1
P2R1A3	160.3 ± 3.6
P2R2A2	158.2 ± 4.8
R6	150.0 ± 4.5

The results obtained confirmed the hydrophobic character of the composites, as well as their base materials (PVB and rubber). All composites showed higher water contact angles than rubber (R6) and PVB (P6); additionally, by analyzing the results, a tendency can be inferred: the higher the aerogel content in the composite, the more hydrophobic the composite is. This is related to the hydrophobic groups of the silica aerogel [38].

#### 2.4. Density and Thermal Conductivity

The influence of the three different components, aerogel, PVB and rubber, on the bulk density was investigated, and the obtained results are given in Figure 3. The denser material, as can be seen in Figure 3, is recycled tire rubber, followed by PVB. However, the

incorporation of aerogel into the composite led to a decrease in the bulk density. This result was expected due to the characteristic low bulk density of aerogels [39]. Therefore, and as expected, the addition and increase in rubber to the composite induced an increase in the bulk density of the composites.

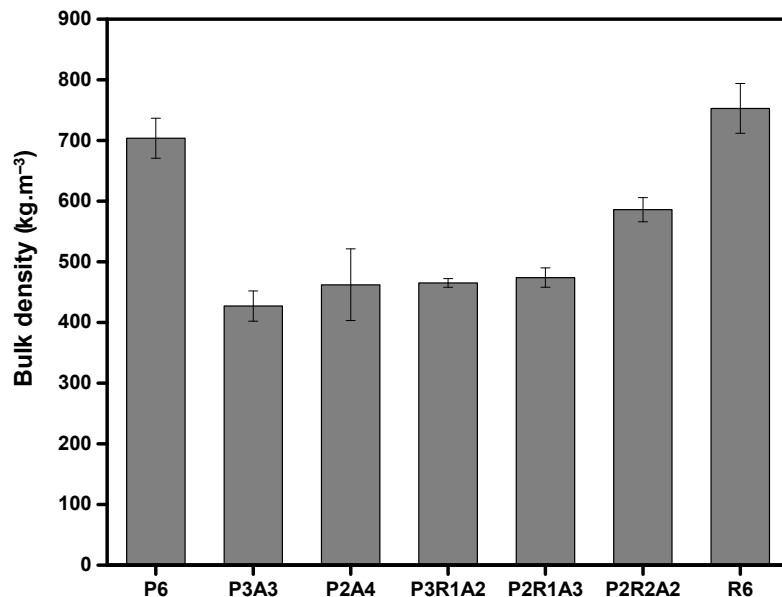


**Figure 3.** Bulk density for different samples.

The thermal conductivity values tendency (Figure 4) agrees with the trend of the bulk density. Generally, both values decrease with aerogel addition due to the increase in porosity [40]. The composite with a lower thermal conductivity value was P3A3 ( $44 \text{ mW}\cdot\text{m}^{-1}\text{K}^{-1}$ ), which does not contain rubber. By adding 1 g of rubber and removing 1 g of PVB from the composite (P2R1A3), the thermal conductivity value remains relatively low, around  $55 \text{ mW}\cdot\text{m}^{-1}\text{K}^{-1}$ , which makes it a great composite candidate for the insulation of buildings.

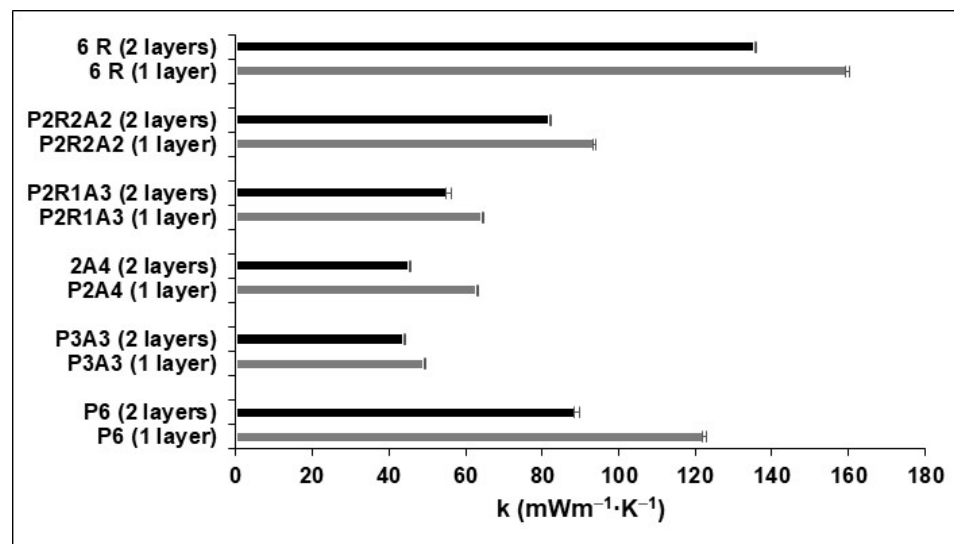


**Figure 4.** Thermal conductivity for single and double layers.

Since the results were promising for P3R1A2, the conductivity of samples with double the thickness was also measured (two samples of the same composite overlaid). The obtained results are also represented in Figure 4, in which a reduction in the conductivity

value that varies between 10 and 30% from single to double layer can be observed for composites without rubber. This reduction was less significant for samples that include the three components: aerogel, PVB and rubber.

### 2.5. Mechanical Characterization

The main purpose of this material is to be used in civil construction applications; therefore, mechanical properties are crucial, in particular the ability of the material to recover after compression. The mechanical behavior of the different samples was assessed by uniaxial compression tests under the same conditions up to the maximum load of the compression cell (2.8 kN) and are presented in Figure 5. Different values of maximum compressive strain were obtained for the tested materials as expected since, in the tests, the strain was not set at a chosen value. The different values observed are related to the different chemical structures of the different components, which can generate different mechanical resistance. Liu et al. [41] divided the mechanical behavior of PVB under quasi-static compression into three different stages similar to our results in Figure 5. In the first region, corresponding to a linear-elastic region, the stress of PVB increases gently along with the strain because of its large particle distances. An increase in stress is observed in the second region, which is likely due to the movement of dislocations [42,43]. In the final stage is present a significant increase in the slope of the stress-strain curve due to the densification of the porous structure, and consequently, the stiffness of the compressed sample increases.

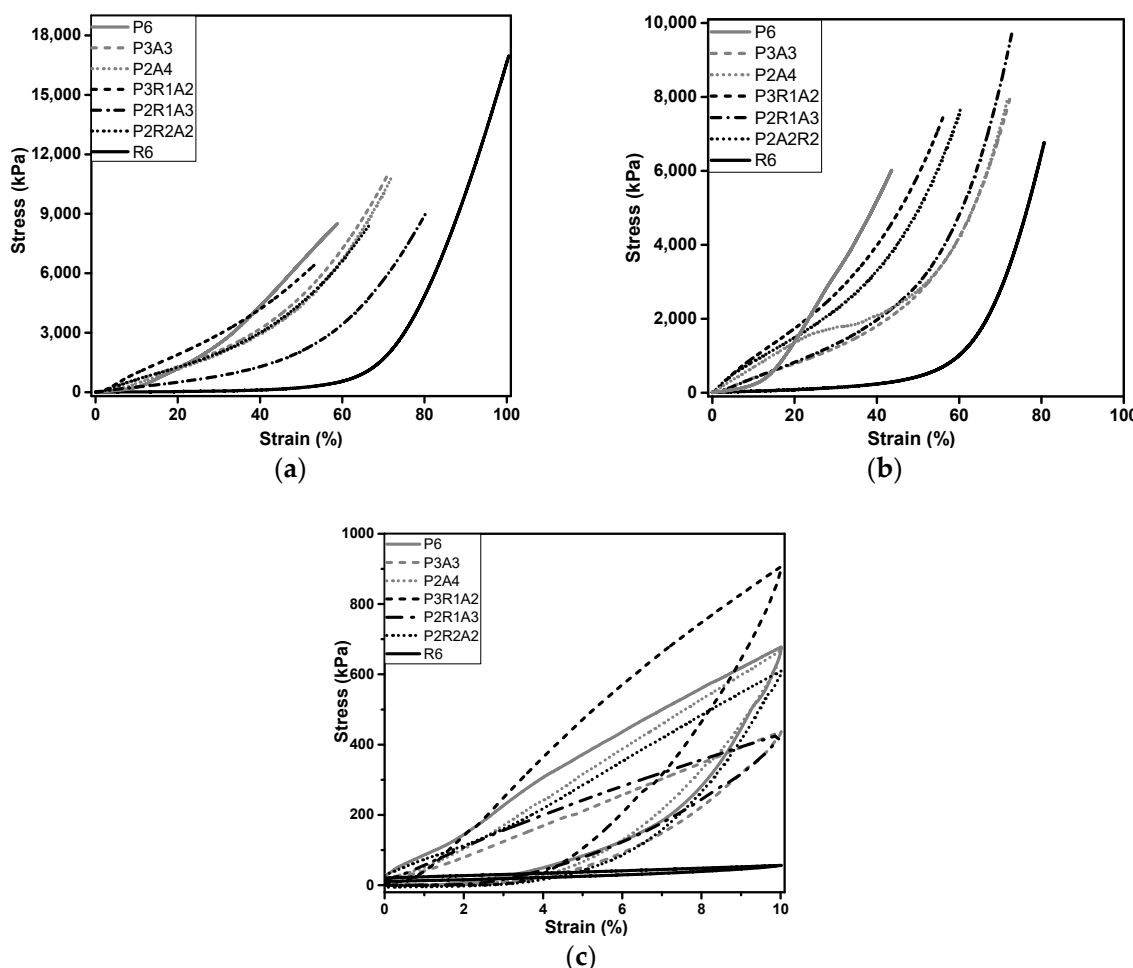


**Figure 5.** Stress–strain curves obtained in uniaxial compression mechanical tests with different compounds tested: up to maximum load of 3 kN for: (a) one-layer samples; (b) two layers samples; and tested (c) under a uniaxial compression–decompression cycle for one-layer samples.

The different values of maximum stress observed between one-layer and two-layer samples were possibly due to slippage between layers.

From the curves in Figure 5, it can be seen that rubber is the least stiff material.

The Young's modulus was evaluated from the linear region of stress-strain loading curve of the compression test, and the results are shown in Table 2. The values obtained have different orders of magnitude among the samples, PVB being the one with the highest value and rubber the lowest value. The greater the Young's modulus, the more rigid the material or the lesser the elastic deformation for the same applied load. All samples analyzed contained PVB with the exception of R6, which contains only rubber. The highest value was obtained for the sample with the higher amount of PVB, i.e., as expected. The introduction of aerogel leads to a decrease in Young's modulus, as is the case of the P3A3 and P2A4 samples. By adding rubber, the value of the Young's modulus decreases even more. The sample with the higher Young's modulus is P2R2A2, making it the more compact and rigid sample.

**Table 2.** Mechanical properties of different samples and composites in single layer.

Samples and Composites	Young's Modulus (kPa)	Compressive Stress after 10% Strain (kPa)	Recovery after 10% of Compression
P6	79.3	978	69
P3A3	75.4	587	84
P2A4	61.9	812	87
P3R1A2	12.9	855	84
P2R1A3	40.8	614	91
P2R2A2	93.2	652	90
R6	4.6	91	98

Recovery tests were performed, and the results indicate that in general, after 10% strain, the samples restore up to 70–98% of their shape (Table 2). These results indicate an excellent mechanical performance of the composites in terms of flexibility. A good capacity of these materials to recover their original shape during unloading is very important considering the construction application.

## 2.6. Surface Morphology

The significant difference obtained in the Young's modulus of the different composites is probably due to the different interaction between PVB, rubber and silica aerogel during processing. To better understand the morphology of the composites, SEM images were recorded and are displayed in Figure 6.

The images show that PVB acts as the binder of the composite since its presence improves the smoothness of the composite along with its homogenous appearance. On the opposite way, rubber sample (R6) shows several agglomerates, inducing an increase in the roughness of the composites with rubber; however, these roughness/agglomerates are more evident with the increase in silica aerogels content in the composites, which might be explained due to the silica aerogels' properties, including the ability to increase porosity [44].

These results are in line with the results obtained from the mechanical tests: PVB is more compact, and it presented the highest value of Young's modulus, rubber has a lower value of Young's modulus, and in the SEM images, we can observe agglomerates.

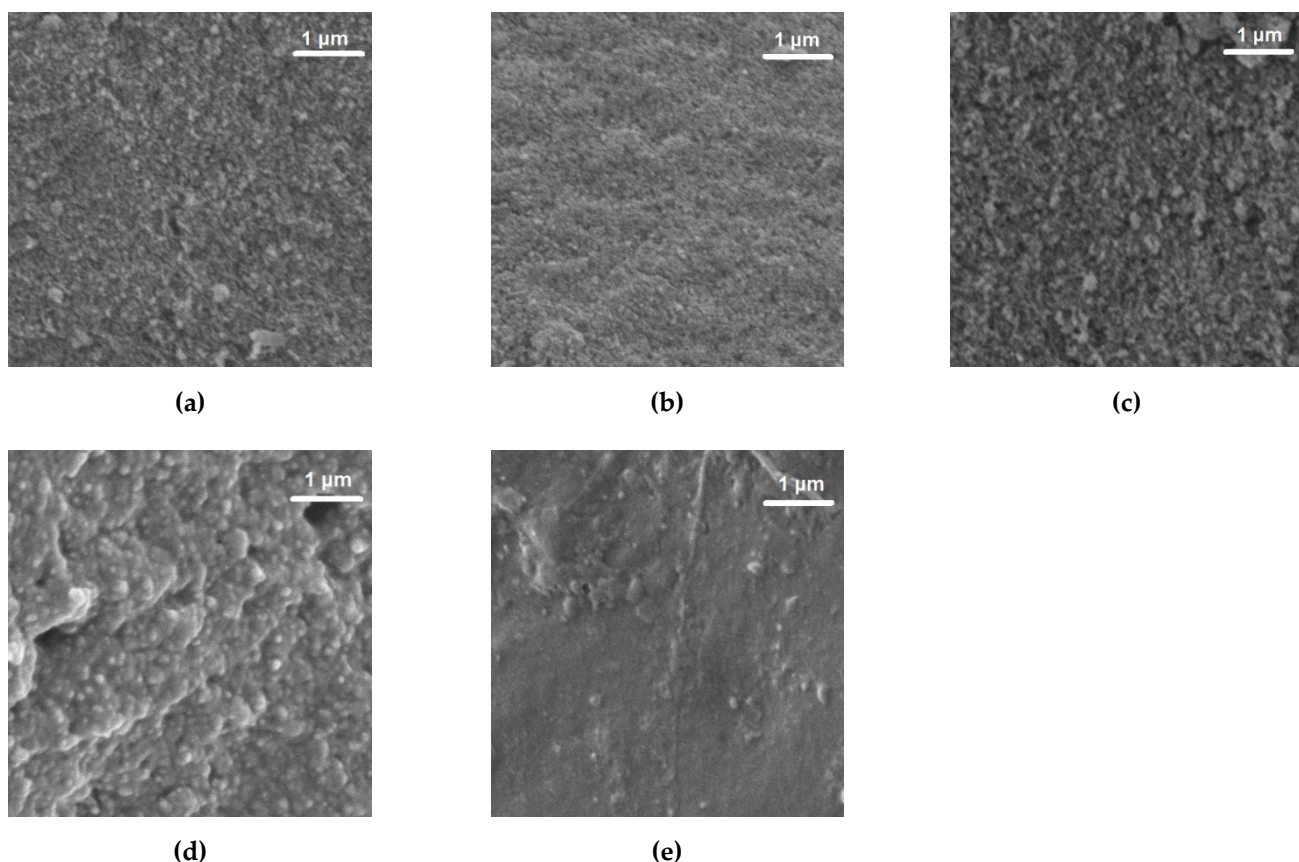


**Figure 6.** SEM images of materials: (a) P2R2A2, (b) P2R1A3, (c) P3A3 and samples (d) R6 and (e) P6.

### 3. Materials and Methods

#### 3.1. Materials

For composite production were used the following materials: tetraethoxysilane (TEOS, purity  $\geq 99\%$ , Aldrich, Portugal,  $\text{Si}(\text{OC}_2\text{H}_5)_4$ ), peracetic acid (38–40%, Merck, Portugal,  $\text{CH}_3\text{CO}_3\text{H}$ ), ethanol (absolute, Fluka, Portugal,  $\text{C}_2\text{H}_5\text{OH}$ ), ammonium hydroxide (25%  $\text{NH}_3$  in  $\text{H}_2\text{O}$ , Fluka Analytical,  $\text{NH}_4\text{OH}$ ), n-hexane (purity  $> 95\%$ , Fisher Chemical, Portugal,  $\text{C}_6\text{H}_{14}$ ), hexamethyldisiloxane (HMDSO, purity  $> 98\%$ , Acros Organics, Portugal,  $(\text{CH}_3)_3\text{SiOSi}(\text{CH}_3)_3$ ), trimethylchlorosilane (TMCS, purity  $\geq 98\%$ , Sigma Aldrich, Portugal,  $(\text{CH}_3)_3\text{SiCl}$ ), polyvinyl butyral (PVB, 60H, Kuraray America, Inc.,  $\text{C}_{14}\text{H}_{24}\text{O}_5$ ) and tire rubber with a diameter  $< 0.8$  mm (provided by Amorim Cork Composites®, Mozelos, Portugal).

#### 3.2. Synthesis of the Aerogel

The first step for the silica aerogel synthesis consisted of the addition of ethanol, TEOS and double-distilled water, with a molar ratio of 10:1:4, and then the mixture was stirred for 30 min. The silica gel was obtained by a low-temperature sol-gel process. The nanostructured solid network of silica is formed as a result of hydrolysis and condensation reactions of the silica precursors, in which siloxane bridges ( $\text{Si}-\text{O}-\text{Si}$ ) are formed. The hydrolysis step involves the conversion of the alkoxide to silanol. The hydrolysis of silicon alkoxides was carried out with a catalyst [7]. A basic solution,  $\text{NH}_4\text{OH}$  2.5 M, was added to the former solution and kept under strong agitation for 1 min. The samples were kept in an oven at 27 °C for 5 days for aging.

The gels were cut into small sizes and washed with ethanol and hexane at 50 °C. The samples were then subjected to a surface modification procedure: sialylation. The sialylating solution comprises hexane, HMDSO and TMCS (70:20:10 v/v%). The gels were immersed in the sialylating solution and then placed in an oven at 50 °C for 6 h. To dry the

gel, the solution was removed, and the gel was kept in the hood for 24 h and then at 100 °C for 3 h and 150 °C for 3 h.

### 3.3. Synthesis of the Aerogel–Rubber Composites

The synthesized aerogel, previously grounded, was mixed with recycled tire rubber and PVB (<0.8 mm), in different mass proportions. The mixture was placed into a metallic mold and was pressed ( $1.03 \times 10^8$  Pa) in a laboratory hydraulic press (Carver Laboratory Press, Model C. 12 ton, heated 6" platens form Carver, Inc., Wabash, USA) for 5 min at 150 °C. The different composites produced (41 mm × 41 mm × 6 mm) are shown in Table 3.

**Table 3.** Sample nomenclature.

Samples	Images	Composition
P6		6 g PVB
P3A3		3 g PVB, 3 g Aerogel
P2A4		2 g PVB, 4 g Aerogel
P3R1A2		3 g PVB 1 g Rubber 2 g Aerogel
P2R1A3		2 g PVB 1 g Rubber 3 g Aerogel
P2R2A2		2 g PVB 2 g Rubber 2 g Aerogel
R6		6 g Rubber

### 3.4. Characterization of the Composites

The properties of aerogel, PVB, tire rubber and final composites were assessed by different characterization techniques. The chemical structure was evaluated by attenuated total reflection (ATR) Fourier-transform infrared spectroscopy (FTIR) (FT/IR 4200, Jasco, Tokyo, Japan) (ATR-FTIR), collecting the spectra between a wavenumber of 4000 and  $400\text{ cm}^{-1}$ , with 128 scans and  $4\text{ cm}^{-1}$  of resolution. The bulk density ( $\rho_b$ ) was determined from the weight and volume of regular pieces of the samples. The degree of hydrophobicity was determined through contact angle measurements by an OCA 20 system (Dataphysics, Filderstadt, Germany) at room temperature using the sessile drop method and high-purity water. Scanning electron microscopy (SEM) images were obtained using a Compact/VPCcompact FESEM (Zeiss Merlin, Leipzig, Germany) microscope after coating the aerogel samples with a thin gold layer by physical vapor deposition for 20 s. Thermal properties were assessed by thermal gravimetric analysis (TGA) and thermal conductivity. The thermal stability of different materials was obtained by using DSC/TGA equipment

(TGA-Q500, TA Instruments, Hüllhorst, Germany), from 20 °C to 800 °C at a 10 °C min<sup>-1</sup> heating rate under nitrogen flow. Thermal conductivity,  $k$ , was measured with a Thermal Constants Analyzer TPS 2500 S (Hot Disk, Göteborg, Sweden), using the transient plane source method with two samples maintained at 20 °C.

#### 4. Conclusions

Samples with silica aerogel, rubber and PVB were successfully prepared using the hot-pressing technique.

The incorporation of recycled rubber into the samples did not lead to a negative impact on the final physical and thermal properties of the material, meaning that the final composites presented thermal conductivity ( $55.5 \pm 0.5 \text{ mW m}^{-1} \text{ K}^{-1}$ ). The three composites showed excellent thermal stability with negligible weight loss up to 400 °C and losses lower than 8.5 wt% up to 600 °C. The addition of rubber also improved the mechanical properties; when compared with samples without rubber, the materials exhibited flexibility. The combination of these properties shows that the composites with aerogel and rubber here developed have the potential to be applied as a thermal insulation material in buildings. The use of small amounts of end-of-life tire rubber for this type of purpose can be a path to reduce it in the environment.

**Author Contributions:** Conceptualization, P.A. and A.D.R.P.; methodology, P.A. and A.D.R.P.; validation, D.A.D., P.A. and A.D.R.P.; formal analysis, D.A.D., P.A. and A.D.R.P.; investigation, D.A.D., P.A. and A.D.R.P.; resources, P.A. and A.D.R.P.; writing—original draft preparation, P.A. and A.D.R.P.; writing—review and editing, P.A. and A.D.R.P.; visualization, D.A.D., P.A. and A.D.R.P.; supervision, P.A. and A.D.R.P.; project administration, P.A. and A.D.R.P.; funding acquisition, P.A. and A.D.R.P. All authors have read and agreed to the published version of the manuscript.

**Funding:** This research was co-funded by European Regional Development Funds (ERDF), through the Operational Programme for Competitiveness and Internationalisation—COMPETE2020, and by national funds through FCT—Foundation for Science and Technology, under the scope of the project POCI-01-0145-FEDER-032061-TYRE4BUILDINS: Recycled Tyre Rubber Resin-Bonded for Building Insulation Systems Towards Energy Efficiency, developed by the University of Coimbra. The authors would like to thank the Strategic Research Centre Project UIDB/00102/2020 and UI/BD/150855/2021, funded by the Fundação para a Ciência e a Tecnologia (FCT).

**Institutional Review Board Statement:** Not applicable.

**Informed Consent Statement:** Not applicable.

**Data Availability Statement:** Data are contained within the article. The raw/processed data required to reproduce these findings cannot be shared at this time due to technical or time limitations but will be sent upon request.

**Acknowledgments:** The authors would like to thank Paulo Santos, from the Institute for Sustainability and Innovation in Structural Engineering of the University of Coimbra, for providing recycled tire rubber used in this work.

**Conflicts of Interest:** The authors declare no conflict of interest.

**Sample Availability:** Samples of the compounds are available from the authors upon request.

#### References

1. Mazrouei-Sebdani, Z.; Begum, H.; Schoenwald, S.; Horoshenkov, K.V.; Malfait, W.J. A review on silica aerogel-based materials for acoustic applications. *J. Non-Cryst. Solids* **2021**, *562*, 120770. [[CrossRef](#)]
2. Ratke, L. Monoliths and Fibrous Cellulose Aerogels. In *Aerogels Handbook. Advances in Sol-Gel Derived Materials and Technologies*; Aegerter, M., Leventis, N., Koebel, M., Eds.; Springer: New York, NY, USA, 2011; pp. 173–190.
3. Feng, Q.; Chen, K.; Ma, D.; Lin, H.; Liu, Z.; Qin, S.; Luo, Y. Synthesis of high specific surface area silica aerogel from rice husk ash via ambient pressure drying. *Colloids Surf. A: Physicochem. Eng. Asp.* **2018**, *539*, 399–406. [[CrossRef](#)]
4. Li, M.; Jiang, H.; Xu, D.; Hai, O.; Zheng, W. Low density and hydrophobic silica aerogels dried under ambient pressure using a new co-precursor method. *J. Non-Cryst. Solids* **2016**, *452*, 187–193. [[CrossRef](#)]

5. Schultz, J.M.; Jensen, K.I.; Kristiansen, F.H. Super insulating aerogel glazing. *Sol. Energy Mater. Sol. Cells* **2005**, *89*, 275–285. [[CrossRef](#)]
6. Carraher, C.E., Jr. Silica aerogels—Properties and uses. *Polym. News* **2005**, *30*, 386–388. [[CrossRef](#)]
7. Gurav, J.L.; Jung, I.-K.; Park, H.-H.; Kang, E.S.; Nadargi, D.Y. Silica Aerogel: Synthesis and Applications. *J. Nanomater.* **2010**, *2010*, 1–11. [[CrossRef](#)]
8. Soares, N.; Santos, P.; Gervásio, H.; Costa, J.J.; Simões da Silva, L. Energy efficiency and thermal performance of lightweight steel-framed (LSF) construction: A review. *Renew. Sustain. Energy Rev.* **2017**, *78*, 194–209. [[CrossRef](#)]
9. Maleki, H.; Durães, L.; Portugal, A. Synthesis of lightweight polymer-reinforced silica aerogels with improved mechanical and thermal insulation properties for space applications. *Microporous Mesoporous Mater.* **2014**, *197*, 116–129. [[CrossRef](#)]
10. Wu, Z.; Zhang, L.; Li, J.; Zhao, X.; Yang, C. Organic-inorganic hybridization for the synthesis of robust in situ hydrophobic polypropylsilsesquioxane aerogels with fast oil absorption properties. *RSC Adv.* **2018**, *8*, 5695–5701. [[CrossRef](#)] [[PubMed](#)]
11. Bhagat, S.D.; Rao, A.V. Surface chemical modification of TEOS based silica aerogels synthesized by two step (acid-base) sol-gel process. *Appl. Surf. Sci.* **2006**, *252*, 4289–4297. [[CrossRef](#)]
12. Linhares, T.; Pessoa De Amorim, M.T.; Durães, L. Silica aerogel composites with embedded fibres: A review on their preparation, properties and applications. *J. Mater. Chem. A* **2019**, *7*, 22768–22802. [[CrossRef](#)]
13. Leventis, N.; Sotiriou-Leventis, C.; Zhang, G.; Rawashdeh, A.-M.M. Nanoengineering Strong Silica Aerogels. *Nano Lett.* **2002**, *2*, 957–960. [[CrossRef](#)]
14. Leventis, N.; Sadekar, A.; Chandrasekaran, N.; Sotiriou-Leventis, C. Click Synthesis of Monolithic Silicon Carbide Aerogels from Polyacrylonitrile-Coated 3D Silica Networks. *Chem. Mater.* **2010**, *22*, 2790–2803. [[CrossRef](#)]
15. Boday, D.J.; Keng, P.Y.; Muriithi, B.; Pyun, J.; Loy, D.A. Mechanically reinforced silica aerogel nanocomposites via surface initiated atom transfer radical polymerizations. *J. Mater. Chem.* **2010**, *20*, 6863–6865. [[CrossRef](#)]
16. Cuce, E.; Cuce, P.M.; Wood, C.J.; Riffat, S.B. Toward aerogel based thermal superinsulation in buildings: A comprehensive review. *Renew. Sustain. Energy Rev.* **2014**, *34*, 273–299. [[CrossRef](#)]
17. Smith, D.M.; Maskara, A.; Boes, U. Aerogel-based thermal insulation. *J. Non-Cryst. Solids* **1998**, *225*, 254–259. [[CrossRef](#)]
18. Gao, T.; Jelle, B.P.; Gustavsen, A.; Jacobsen, S. Aerogel-incorporated concrete: An experimental study. *Constr. Build. Mater.* **2014**, *52*, 130–136. [[CrossRef](#)]
19. Gao, T.; Jelle, B.P.; Ihara, T.; Gustavsen, A. Insulating glazing units with silica aerogel granules: The impact of particle size. *Appl. Energy* **2014**, *128*, 27–34. [[CrossRef](#)]
20. Gao, T.; Jelle, B.P.; Gustavsen, A.; He, J. Lightweight and thermally insulating aerogel glass materials. *Appl. Phys. A* **2014**, *117*, 799–808. [[CrossRef](#)]
21. Roque, E.; Santos, P.; Pereira, A.C. Thermal and sound insulation of lightweight steel-framed façade walls. *Sci. Technol. Built Environ.* **2018**, *25*, 156–176. [[CrossRef](#)]
22. Roque, E.; Santos, P. The Effectiveness of Thermal Insulation in Lightweight Steel-Framed Walls with Respect to Its Position. *Buildings* **2017**, *7*, 13. [[CrossRef](#)]
23. Grammelis, P.; Margaritis, N.; Dallas, P.; Rakopoulos, D.; Mavrias, G. A Review on Management of End of Life Tires (ELTs) and Alternative Uses of Textile Fibers. *Energies* **2021**, *14*, 571. [[CrossRef](#)]
24. Thai, Q.B.; Siang, T.E.; Le, D.K.; Shah, W.A.; Phan-Thien, N.; Duong, H.M. Advanced fabrication and multi-properties of rubber aerogels from car tire waste. *Colloids Surf. A: Physicochem. Eng. Asp.* **2019**, *577*, 702–708. [[CrossRef](#)]
25. Sienkiewicz, M.; Janik, H.; Borzędowska-Labuda, K.; Kucińska-Lipka, J. Environmentally friendly polymer-rubber composites obtained from waste tyres: A review. *J. Clean. Prod.* **2017**, *147*, 560–571. [[CrossRef](#)]
26. Bowles, A.; Fowler, G.; O'Sullivan, C.; Parker, K. Sustainable rubber recycling from waste tyres by waterjet: A novel mechanistic and practical analysis. *Sustain. Mater. Technol.* **2020**, *25*, e00173. [[CrossRef](#)]
27. Walters, M.H.; Keyte, D.N. Heterogeneous Structure in Blends of Rubber Polymers. *Rubber Chem. Technol.* **1965**, *38*, 62–75. [[CrossRef](#)]
28. Zhang, X.; Hao, H.; Shi, Y.; Cui, J. The mechanical properties of Polyvinyl Butyral (PVB) at high strain rates. *Constr. Build. Mater.* **2015**, *93*, 404–415. [[CrossRef](#)]
29. Chen, S.; Chen, X.; Wu, X. The mechanical behaviour of polyvinyl butyral at intermediate strain rates and different temperatures. *Constr. Build. Mater.* **2018**, *182*, 66–79. [[CrossRef](#)]
30. Ismail, A.A.; van de Voort, F.R.; Sedman, J. Chapter 4 Fourier transform infrared spectroscopy: Principles and applications. *Tech. Instrum. Anal. Chem.* **1997**, *18*, 93–139. [[CrossRef](#)]
31. Hajian, M.; Reisi, M.R.; Koohmreh, G.A.; Jam, A.R.Z. Preparation and characterization of Polyvinylbutyral/Graphene Nanocomposite. *J. Polym. Res.* **2012**, *19*, 9966. [[CrossRef](#)]
32. Yang, B.; Ni, H.; Huang, J.; Luo, Y. Effects of Poly(vinyl butyral) as a Macromolecular Nucleating Agent on the Nonisothermal Crystallization and Mechanical Properties of Biodegradable Poly(butylene succinate). *Macromolecules* **2013**, *47*, 284–296. [[CrossRef](#)]
33. Rolere, S.; Liengprayoon, S.; Vaysse, L.; Sainte-Beuve, J.; Bonfils, F. Investigating natural rubber composition with Fourier Transform Infrared (FT-IR) spectroscopy: A rapid and non-destructive method to determine both protein and lipid contents simultaneously. *Polym. Test.* **2015**, *43*, 83–93. [[CrossRef](#)]
34. Gunasekaran, S.; Natarajan, R.; Kala, A. FTIR spectra and mechanical strength analysis of some selected rubber derivatives. *Spectrochim. Acta Part A Mol. Biomol. Spectrosc.* **2007**, *68*, 323–330. [[CrossRef](#)]

35. Al-Oweini, R.; Rassy, H. Synthesis and characterization by FTIR spectroscopy of silica aerogels prepared using several  $\text{Si(OR)}_4$  and  $\text{R''Si(OR')}_3$  precursors. *J. Mol. Struct.* **2020**, *919*, 140–145. [[CrossRef](#)]
36. Chen, F.; Qian, J. Studies of the thermal degradation of waste rubber. *Waste Manag.* **2003**, *23*, 463–467. [[CrossRef](#)]
37. Kang, S.-K.; Choi, S.-Y. Synthesis of low-density silica gel at ambient pressure: Effect of heat treatment. *J. Mater. Sci.* **2000**, *35*, 4971–4976. [[CrossRef](#)]
38. Malfait, W.J.; Zhao, S.; Verel, R.; Iswar, S.; Rentsch, D.; Fener, R.; Zhang, Y.; Milow, B.; Koebel, M.M. The Surface Chemistry of Hydrophobic Silica Aerogels. *Chem. Mater.* **2015**, *27*, 6737–6745. [[CrossRef](#)]
39. Lamy-Mendes, A.; Silva, R.F.; Durães, L. Advances in carbon nanostructure–silica aerogel composites: A review. *J. Mater. Chem. A* **2017**, *6*, 1340–1369. [[CrossRef](#)]
40. Maleki, H.; Durães, L.; Portugal, A. An overview on silica aerogels synthesis and different mechanical reinforcing strategies. *J. Non-Crystalline Solids* **2014**, *385*, 55–74. [[CrossRef](#)]
41. Liu, B.; Sun, Y.; Li, Y.; Wang, Y.; Ge, D.; Xu, J. Systematic experimental study on mechanical behavior of PVB (polyvinyl butyral) material under various loading conditions. *Polym. Eng. Sci.* **2012**, *52*, 1137–1147. [[CrossRef](#)]
42. Hosford, W.F. *Mechanical Behavior of Materials*, 2nd ed.; Cambridge University Press: New York, NY, USA, 2010.
43. Ishida, T.; Kakushima, K.; Mizoguchi, T.; Fujita, H. Role of dislocation movement in the electrical conductance of nanocontacts. *Sci. Rep.* **2012**, *2*, 21–24. [[CrossRef](#)] [[PubMed](#)]
44. Pajonk, G.M.; Rao, A.V.; Parvathy, N.N.; Elaloui, E. Microstructural characterization of silica aerogels using scanning electron microscopy. *J. Mater. Sci.* **1996**, *31*, 5683–5689. [[CrossRef](#)]